widths seem to be reduced at 300°K by motional narrowing. The observed linewidth is separated into its separate contributions. The linear field dependence of the width (Fig. 5) is attributed primarily to anisotropic Knight-shift broadening, although inhomogeneous isotropic Knight-shift broadening is not excluded. The rapid increase of the zero-field linewidth upon alloying is attributed to a combination of indirect spin exchange and pseudodipolar coupling. These interactions are also responsible for the line shape change from Lorentzian toward Gaussian. The exchange-only second moment yields a value for the near-neighbor exchange constant for unlike nuclei $h^{-1}|A_{\mathrm{Pb-In}}|=0.9\pm0.4$ kc/sec. The pure lead line is Lorentzian due to exchange narrowing. A second-moment analysis yields a value for the strength of the interaction between like nuclei, $h^{-1}|A_{\mathrm{Pb-Pb}}|=1.4$ kc/sec. The pseudodipolar exchange constant is found to be $h^{-1}|B_{\mathrm{Pb-In}}|=1.0\pm0.2$ kc/sec. Large values for the ratio $B_{\mathrm{Pb-In}}/A_{\mathrm{Pb-In}}$ and the ratio of pseudodipolar to classical dipolar indicate that the amount of p character probably greatly exceeds the amount of s character in the electron wave functions at the Fermi surface in these alloys, and is consistent with the observation of anisotropic Knight-shift broadening.

ACKNOWLEDGMENTS

We are indebted to the Consolidated Mining and Smelting Company of Canada Limited for the preparation of the lead-indium alloy powders.

PHYSICAL REVIEW VOLUME 132, NUMBER 4 15 NOVEMBER 1963

Infrared Lattice Vibrations and Dielectric Dispersion in Corundum

A. S. BARKER, JR.
Bell Telephone Laboratories, Murray Hill, New Jersey
(Received 1 July 1963)

Room-temperature reflectivity measurements in the wavelength range 1 to 140 μ have been made on corundum and ruby. Classical oscillator analysis of the data shows that the optical lattice modes with dipole moment vibrating perpendicular to the C axis occur at 15.7, 17.6, 22.6, 26.0 μ. Those vibrating parallel to the C axis occur at 17.1 and 25.0 μ. The line-widths and strengths are reported. Many forbidden modes are observed. Two of these can have a strength which is comparable to the allowed modes but which is sensitive to surface treatment. Symmetry arguments show that these strong forbidden modes are the A_{1u} (forbidden) phonon branches picking up dipole moment as a result of shear strain.

INTRODUCTION

THE infrared lattice-vibration spectra of corundum (α-Al_2O_3) and chromium-doped corundum (ruby) have been studied by several workers since the original work of Coblentz[1] in 1908. Krishnan has reported on the Raman spectrum of alumina[2] and summarized the infrared results to 1947.[3] In spite of the large body of experimental results listed by Krishnan, and some more very recent and extensive infrared measurements,[3,4] there are several ambiguities and anomalies in the frequencies assigned by the various authors. Also, all of the infrared active modes predicted by group theory have not been previously identified experimentally.

The present work was undertaken to discover all the normally allowed infrared vibration modes of the α-Al_2O_3 lattice and to obtain the optical constants throughout the region of the lattice vibrations. Polarized reflection spectra were made from 1 to 140 μ and these spectra were analyzed using Kramers-Kronig dispersion analysis and classical oscillator formulas.[5]

Four infrared modes active for $E\perp C$ axis and two active for $E\|C$ axis are predicted by the symmetry of the α-Al_2O_3 lattice where E is the electric field vector of the infrared beam. These modes are clearly detected in the present experiments and are discussed below. Anomalously low-frequency modes at 194 cm^{-1} and 244 cm^{-1} were reported by Parodi,[6] and have been used by several authors to explain fine structure which appears in the luminescence spectrum of ruby.[3,7,8] No infrared modes were found at these frequencies in the present work. As might be expected, the measurements show that the presence of chromium impurities even up

[1] W. W. Coblentz, *Supplementary Investigations of Infrared Spectra* (The Carnegie Institution, Pub. No. 97, Washington, 1908), p. 17.
[2] Various names are used in the literature to describe pure α-Al_2O_3 crystals. Some of these are: Corundum, sapphire, and alumina (or better-α-alumina).
[3] R. S. Krishnan, Proc. Indian Acad. Sci. **26A**, 450 (1947).
[4] A. Mitsuishi, H. Yoshinaga, S. Fujita, and Y. Suemoto, J. Appl. Phys. (Japan) **1**, 1 (1962).
[5] W. G. Spitzer and D. A. Kleinman, Phys. Rev. **121**, 1324 (1961).
[6] M. Parodi, Compt. Rend. **205**, 906 (1937).
[7] R. A. Ford and O. F. Hill, Spectrochim. Acta, **16**, 493 (1960).
[8] It seems likely that phonons near the zone boundaries will contribute most strongly to the luminescence structure, thus, infrared and Raman frequencies may not be very useful in fitting such structure.

TABLE I. Samples and spectra.

	Sample and source	C axis	Spectra
No. 1	1.0×1.0×0.3 cm. Cut from Linde flame fusion white sapphire boule	Parallel to one of 1 cm edges	$E\perp C$ 1–30 μ $E\|\|$ 1–30 μ
No. 2	1.0×1.0×0.3 cm. Same as No. 1	Perpendicular to large face	$E\perp C$ 1–35 μ (unpolarized)
No. 3	1.59×1.27×0.32 cm. Cut from Meller flame fusion white sapphire boule	Parallel to longest edge	$E\|\|C$ 1–62 μ $E\perp C$ 1–31 μ
No. 4	1.59×1.59×0.32 cm. Same as No. 3	Perpendicular to largest face	$E\perp C$ 1–140 μ (unpolarized)
No. 5	1.26×1.26×0.39 cm. Cut from Linde flame fusion ruby disk 1.8×10^{19} Cr/cc	Parallel to one of the long edges	$E\perp C$ 1–31 μ (unpolarized) $E\perp C$ 10–24 μ $E\|\|C$ 1–34 μ
No. 6	1.48×1.48×0.50 cm. Cut from Linde flame fusion ruby disk 1.8×10^{18} Cr/cc	Parallel to one of the long edges	$E\perp C$ 1–31 μ (unpolarized) $E\perp C$ 10–24 μ $E\|\|C$ 1–34 μ
No. 7	2.0 cm. diam×0.05 cm thick disk cut from boule 2.4×10^{20} Cr/cc	Parallel to the large face	$E\perp C$ 1–30 μ $E\|\|C$ 10–24 μ
No. 8	~1×1×1 cm Flux grown ruby. Natural optically flat faces {0001}, {10$\bar{1}$2}. 0.9×10^{18} Cr/cc	Perpendicular to the {0001} faces	$E\perp C$ 1–30 μ $E\perp C$ 10–24 μ (unpolarized)

to 2.4×10^{20} ions per cc is not detectable in the infrared spectrum.

In the course of the experimental work, it was found that most sapphire samples exhibit many more modes in the infrared spectrum than are allowed by the symmetry of the structure. To study such forbidden modes, many samples of sapphire and ruby from different sources were analyzed. The two strongest forbidden modes in some samples have a strength comparable to the allowed modes. These modes were extensively studied and arguments are presented concerning their appearance and probable symmetry type. The frequencies of the strong modes and many of the much weaker forbidden modes are tabulated below.

EXPERIMENTAL WORK AND ANALYSIS

I. Observation of Allowed Modes

The α-Al_2O_3 lattice belongs to the trigonal crystal system, and, hence, any macroscopic 2nd-rank-tensor property such as the dielectric constant (ϵ) will have two independent parts.[9] Two independent measurements of ϵ, one with the electric vector, E, along the crystalline C axis and the other with the E vector anywhere in the plane perpendicular to the C axis, will completely specify the dielectric tensor. Such pairs of measurements must be made at many frequencies throughout the infrared, since ϵ has a frequency dependence which reflects the spectrum of optically active lattice vibrations.

Room temperature polarized reflection spectra have been taken from 8 samples of sapphire and ruby in the wavelength region 1 to 140 μ. Various faces of each sample were studied and transmission polarizers were used to select the reflectivity for $E\perp C$ axis and $E\|C$ axis. A prism spectrometer was used in the region 1 to 35 μ and a conventional grating spectrometer for the region 30 to 140 μ. The prism spectrometer used, and the general method of taking data have been discussed elsewhere.[5] The samples used are listed in Table I.

The first measurements made on samples 1 and 2 showed gross differences in the $E\perp C$ spectra taken for different crystal cuts. That is, it made considerable difference whether the C axis lay in the reflecting face or was perpendicular to the face when the $E\perp C$ measurement was made. Such discrepancies in optical constants have not been reported before. Attempts were made to attribute the differences to experimental methods, but without success. Samples 1 and 2 were

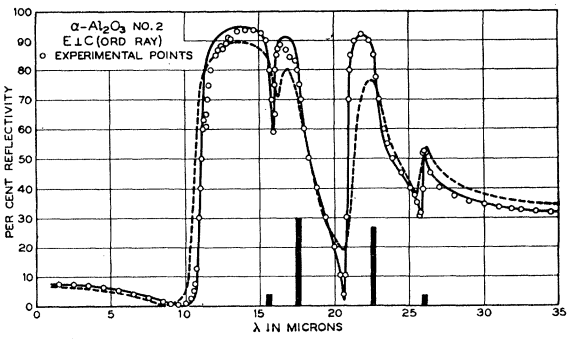

FIG. 1. Reflectivity of Al_2O_3 at room temperature for the electric vector perpendicular to the C axis. The dashed curve shows the first classical oscillator fit to the reflectivity points. The solid curve is the best fit (see text). In this and following figures, the vertical bars indicate the transverse mode frequencies and strengths. A mode strength of $\Delta\epsilon=1$ is given an ordinate of 10% reflectivity.

[9] C. S. Smith, *Solid State Physics* (Academic Press Inc., New York, 1958), Vol. 6. The space dependence of ϵ is being discussed here; each spatial component has of course a real and imaginary part in addition.

TABLE II. Classical oscillator parameters for Al_2O_3.

	ν_i(cm^{-1})	$\lambda_i(\mu)$	$\Delta\epsilon_i$	γ_i/ν_i	ν_l(longitudinal mode)
			$E\perp C$ (ordinary ray) sample #2 unpolarized		
Mode 1	385±1%	26.0	0.30±15%	0.015±25%	388±1%
Mode 2	442±1%	22.6	2.7 ±4%	0.010±15%	480±1%
Mode 3	569±1%	17.6	3.0 ±15%	0.020±15%	625±1%
Mode 4	635±1%	15.7	0.30±20%	0.020±20%	900±1%
		$\epsilon_\infty=3.2$		$\epsilon_\infty+\sum_i \Delta\epsilon_i=9.5$[a]	
			$E\|\|C$ (extraordinary ray) sample #6		
Mode 1	400±1%	25.0	6.8 ±4%	0.020±20%	512±1%
Mode 2	583±1%	17.1	1.7 ±4%	0.035±12%	871±1%
Most (f) prominent forbidden mode	654±1%	15.3	0.04±15%	0.06 ±25%	···
		$\epsilon_\infty=3.1$		$\epsilon_\infty+=\sum_i \Delta\epsilon_i=11.64$[a]	

$E\perp C$ sample 1 (forbidden modes f present)

Mode 1	385	26.0	0.3	0.012
Mode 2	436	22.9	1.1	0.010
Mode 2f	448	22.3	1.6	0.012
Mode 3	571	17.5	1.0	0.015
Mode 3f	598	16.7	2.0	0.060
Mode 4	637	15.7	0.3	0.015

frequencies of other weak forbidden modes

$E\|\|C$		$E\perp C$	
806 cm^{-1}	12.4 μ	889 cm^{-1}	11.25 μ
770	13.0	794	12.6
650	15.4	715	14.0
592	16.9	424	23.6
483	20.7		
472	21.2		
459	21.8		
450	22.2		
439	22.8		

[a] This sum of mode strengths compares favorably with the low-frequency dielectric constants; $\epsilon(0)_\perp=9.35$ and $\epsilon(0)_{||}=11.6$. S. Roberts and D. D. Coon, J. Opt. Soc. Am. **52**, 1023 (1962).

reoriented (C axis determined to within $\frac{1}{2}°$), reground, and polished. Only minor changes resulted from this treatment. Other samples were obtained and were found to exhibit the extra modes also. Since it seems desirable to present the infrared-allowed modes first, certain spectra with strong forbidden modes are not discussed here but are left for a later section.

Figure 1 shows the reflection spectrum of sample 2 for $E\perp C$. It can be seen that there are four strong modes present. This reflection spectrum was transformed using the Kramers-Kronig integral to obtain the reflection phase shift. Using the phase shift and the reflection itself, the real and imaginary parts of the $E\perp C$ dielectric constant $\epsilon_\perp=\epsilon_\perp'-i\epsilon_\perp''$ were calculated at two hundred points in the region 1 to 140 μ.[5,10,11] The graph of $\epsilon''(\nu)$ so obtained showed four peaks or modes at the frequencies 380, 440, 570, and 630 cm^{-1}. Rough measurements were made on the $\epsilon''(\nu)$ graph of the width at half maximum of each peak, and of the area under each peak. These numbers then served as initial values of the classical oscillator parameters to be used in calculating $\epsilon_\perp(\nu)$ of the crystal. The process of fitting now began. Without further reference to the graph of $\epsilon_\perp''(\nu)$, the reflectivity $R_\perp(\nu)$ calculated from the classical oscillator parameters was compared with the measured reflectivity and corrections made to the parameters to improve the fit. A similar analysis was applied to $E||C$ data; typical formulas are given below. Subscripts ($\perp$ or $||$) can be added to all the quantities except ν in applying the formulas to a trigonal crystal such as sapphire

$$\epsilon=\epsilon'-i\epsilon''=\epsilon_\infty+\sum_n \Delta\epsilon_n\nu_n^2/(\nu_n^2-\nu^2+i\nu\gamma_n),$$

$$R=\left|\frac{\sqrt{\epsilon}-1}{\sqrt{\epsilon}+1}\right|^2.$$

The classical oscillator parameters are $\Delta\epsilon_n$, ν_n, γ_n—the strength, frequency, and linewidth of the nth mode, respectively. ϵ_∞ is the limiting value of ϵ at frequencies

[10] A. S. Barker, Jr., and M. Tinkham, Phys. Rev. **125**, 1527 (1962).

[11] W. G. Spitzer, R. C. Miller, D. A. Kleinman, and L. E. Howarth, Phys. Rev. **126**, 1710 (1962).

much greater than the lattice vibration frequencies. R is the power reflectivity at normal incidence. In the calculations described above for fitting calculated and measured reflectivities, the full Fresnel formulas are actually used. These formulas take into account the actual angle of incidence used in the experiments and the angle of the electric vector relative to the plane of incidence.

To illustrate the kind of adjustments that must be made, Fig. 1 shows a dashed curve resulting from the first estimate of the classical oscillator parameters. The solid curve results from the parameters finally adopted after about 10 trials. By the tenth trial, the mode frequencies are known to better than 1 percent.

Figure 2 shows the $E\|C$-axis reflectivity of sample 6. The solid curve is again the classical oscillator fit obtained in this case using two strong modes and one much weaker mode to roughly fit the strongest of the forbidden modes which appear.

The classical fits shown in Figs. 1 and 2 are felt to be about as good as can be obtained without the introduction of extra weak modes. The mode assignment is listed in Table II. Uncertainties are shown for the classical parameters in Table II. The meaning of these uncertainties is that deviation by the amount shown produced a noticeably poorer fit. A more accurate description of the uncertainties is hard to give, however, because of the complicated and nonindependent way each parameter determines the shape of the curve. There is good agreement between our spectra and those of Mitsuishi *et al.* in the cases where the latter used polarizers.[4] A direct comparison with the frequencies obtained by these workers is not very significant since they have tabulated only the transmission minima and reflectivity shoulders without any correction for dispersion. Their paper also has the $E\perp C$ and $E\|C$ spectra reversed, confusing the lattice mode assignments.

The longitudinal mode frequencies ν_l are also listed in the table. These are taken from the zeros of ϵ' evaluated from the classical parameters. The damping of all modes is set to zero to facilitate finding the zeros. A consideration of the frequency shift of the longitudinal vibrations arising from damping indicates that the values of ν_l given are accurate to better than 1% without any adjustment.

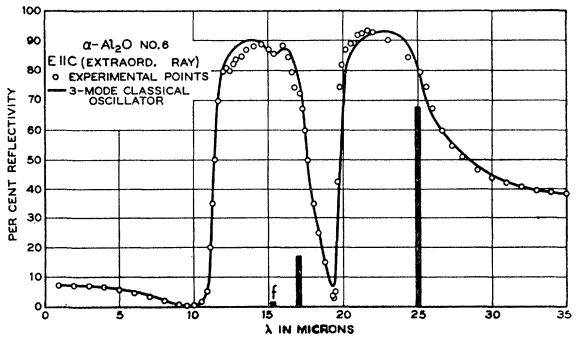

FIG. 2. Reflectivity of Al_2O_3 for $E\|C$ axis. The solid curve was calculated from the classical oscillator formulas using the parameters in Table II. f designates a weak forbidden mode.

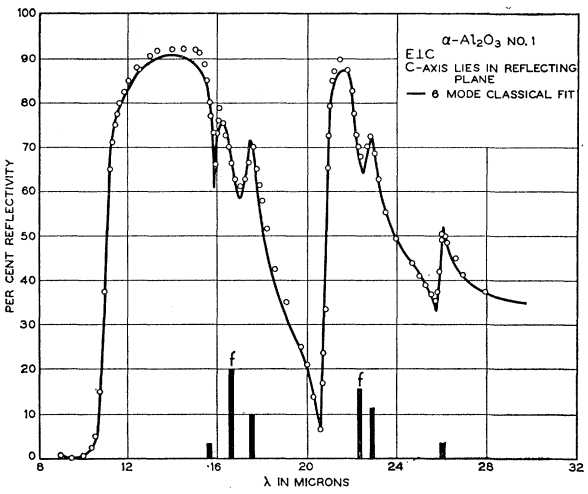

FIG. 3. $E\perp C$ reflectivity of Al_2O_3 taken with a polarizer on a face parallel to the C axis. The two forbidden modes which appear are labeled f. The solid curve was calculated using the parameters in Table II.

All the samples showed some signs of extra dips or anomalous curvature in the reflectivity spectrum indicating extra modes. The fits discussed above can be considerably improved by considering additional weaker modes in the classical oscillator formula for ϵ. Good fits to the reflectivity of other insulators have been obtained in this manner and sometimes there is independent evidence for assigning the extra modes. The addition of extra modes was studied in the present work only for the case of the very strong and easily observed forbidden modes.

II. Observation of Forbidden Modes

Figure 3 shows the $E\perp C$-axis reflection spectrum of sample 1. This spectrum is taken with a polarized beam and the C axis perpendicular to the beam but lying *in* the reflecting surface. The two methods of taking an $E\perp C$ spectrum must be distinguished for sapphire, because of the unusual effects which we are now describing. The spectrum previously shown in Fig. 1, was taken on a crystal face that had the C axis perpendicular to the surface [a {0001} plane] and, hence, required no polarization of the beam. A comparison of Fig. 3 with Fig. 1 shows that there are two extra modes present at about 17 and 22.3 μ. All samples (except #8) studied with $E\perp C$ axis for a face not perpendicular to the C axis showed some sign of the two extra modes. Sample 8, a ruby grown from a flux by J. P. Remeika, became available part way through this study. This ruby exhibited little or no anomalous biaxial behavior in the visible and had natural, optically flat faces which required no polishing for infrared measurements. In

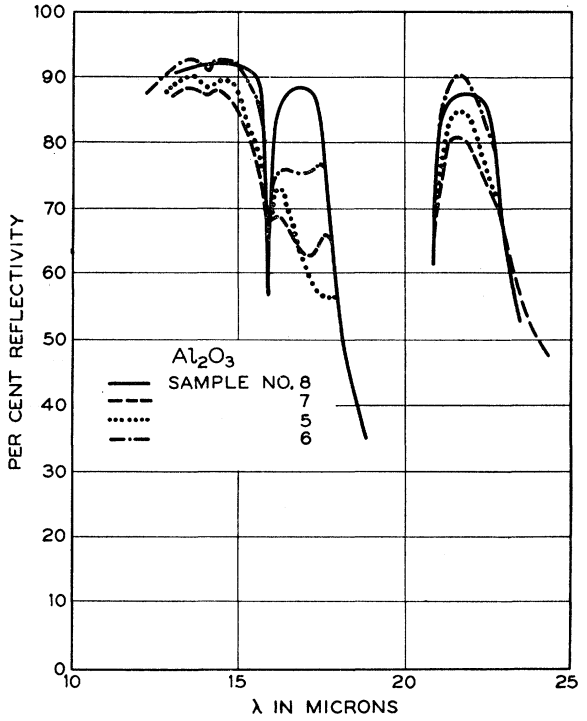

FIG. 4. Reflectivities of several samples of Al_2O_3 measured with $E \perp C$ axis. The reflectivity was measured on a face parallel to the c axis for samples 5, 6, and 7 and on a (10$\bar{T}$2) face for sample 8. All but sample 8 show signs of strong forbidden modes near 16.7 and 22.3 μ.

both these respects it differed from all the other samples studied. Sample 8 showed little or no sign of the extra modes.

In Fig. 3, the solid curve is a classical fit to the reflection spectrum. The classical parameters are listed in Table II. We note that the extra modes are quite comparable in strength to the allowed modes.

Figure 4 shows the appearance, in reflection, of the extra modes in some of the other samples. Sample 8 with no extra modes is shown for comparison. The extra modes vary in strength, from sample to sample and sometimes exhibit high damping (as determined by rough classical oscillator fits). The higher damping makes the modes somewhat harder to see in the reflection spectrum.

Early in the study it was thought that the extra modes added extra oscillator strength to the dielectric constant.[12] Such behavior would explain the anomalous behavior of the index of refraction in the far infrared reported by others for sapphire.[13] Careful fitting of the data in Fig. 3 has shown, however, that there is a type of sum rule operating here. The sum of the strengths of the extra mode at 598 cm^{-1} and the allowed mode at 571 must add to about 3.0 for a good fit. We note that 3.0 is the strength of the allowed mode itself in the case when no extra modes are present (Table II). Similarly, the modes near 436 and 448 cm^{-1} must have a combined strength of about 2.7.

Certain arguments (to be presented below) suggest that the extra modes seen here are not connected directly with anharmonicity (i.e., are not combination bands) but are the result of strain relaxing certain selection rules. Anticipating this, we now start calling these modes *forbidden* modes. Attempts were made to change the strength of the forbidden modes with a mechanically applied stress. A uniaxial stress of about 1000 lbs/cm^2 was applied to sample 1. This stress was sufficient to change the appearance of the anomalous biaxial pattern observed with crossed polaroids. No changes were noted in the reflection spectrum.

Surface strains were considered next. An etch of molten boron oxide and lead oxide was used to remove a few microns from the surfaces of samples 3 and 5. Spectacular changes resulted. Etching the surface removes nearly all trace of the forbidden modes. Grinding with diamond dust by the usual techniques then caused the modes to reappear. Grinding with coarse grit (15-μ particle size) caused the forbidden modes to reappear with large strength. Further grinding with 6-μ grit weakened the forbidden modes. Figures 5 and 6 show these effects.

THEORY AND DISCUSSION

Bhagavantam and Venkatarayudu[14] have studied the symmetry of the lattice vibrations of α-Al_2O_3 for zero wave vector k. Their paper lists the types of symmetry modes and the selection rules for infrared and Raman

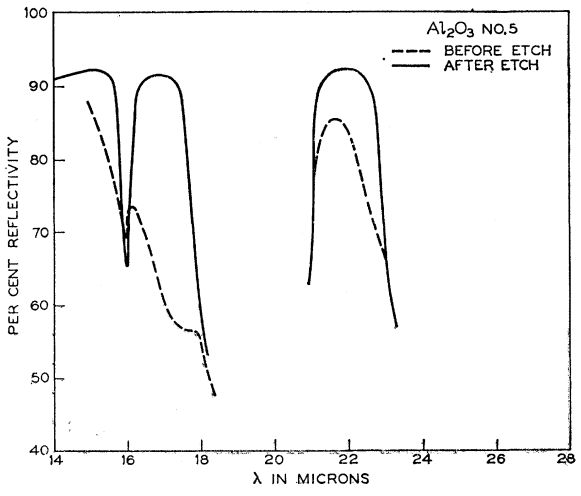

FIG. 5. Reflectivity of an Al_2O_3 sample for $E \perp C$ axis before and after etching treatment. The measurements shown by the solid curve indicate almost complete elimination of interaction with the forbidden phonon modes.

[12] A. S. Barker, Jr. and L. E. Howarth, Bull. Am. Phys. Soc. 8, 194 (1963).
[13] E. V. Loewenstein, J. Opt. Soc. Am. 51, 108 (1961).
[14] S. Bhagavantam and T. Venkatarayudu, Proc. Indian Acad. Sci. 9A, 224 (1939).

TABLE III. Symmetry modes and selection rules for corundum.

Space group D_3^6d		Point group operations E	$3C_2$	$2C_3$	i	$3iC_2$	$2iC_3$	Modes at $k=0$ Acoustic	Optic	Selection rules
	A_{1g}	1	1	1	1	1	1		2	R
	A_{1u}	1	1	1	−1	−1	−1		2	
Irreducible	A_{2g}	1	−1	1	1	−1	1		3	
Representations	A_{2u}	1	−1	1	−1	1	−1	1	2	$IR(E\|\|C)$
	E_g	2	0	−1	2	0	−1		5	R
	E_u	2	0	−1	−2	0	1	1	4	$IR(E\perp C)$
Representation for general cartesian displacement of all atoms.		30	−2	0	0	0	0	Selection rules R=Allowed raman transition IR=Allowed IR transition		

transitions. The results of such a symmetry study are shown in Table III. We note that α-Al_2O_3 has some modes that are neither Raman nor infrared active.

Group theory predicts 4 distinct modes with dipole moment oscillating perpendicular to the C axis. The Coulomb interaction splits the degeneracy between the longitudinal and transverse vibrations for these modes. A study of such Coulomb effects can conveniently be made using Huang's[15] macroscopic theory of long-wave optical vibrations extended to several modes. Table II lists the four frequencies of transverse vibration (or equivalently, the frequencies for infrared absorption in very thin specimens) and the four frequencies for longitudinal vibrations for these modes as deduced from the data. Group theory predicts two distinct modes with dipole moment oscillating parallel to the C axis. Table II shows the actual frequencies and other parameters for these modes also.

The forbidden modes we observe in α-Al_2O_3 are apparently connected with the surface and are strongly influenced by mechanical polishing. It might be argued that these modes are just the result of bond-strength changes in a thin damaged surface layer, which the infrared beam detects along with the regular allowed modes in the crystal below this surface layer. We note that the reflectivity fit requires actual separate extra modes. Thus, a damaged layer theory would seem to require a rather strange surface layer whose anomalous properties do not taper off as one passes from the surface to the interior.

The question arises as to whether these modes are combination bands. It appears rather hard to invoke anharmonic effects here when it is realized that for various crystal cuts and surface treatments, the extra modes vary by a factor of at least 100. An argument can be made connecting the strength of a combination mode and the third (or higher) derivative of the interatomic potential using the concept of a frequency-dependent damping constant. The large variations in the strength of the extra modes would require very large changes in atomic spacing. In addition with an anharmonic theory, one would probably be at a loss to explain why the original allowed modes are not excessively damped by the same mechanism that produces the combination modes.

We now examine arguments that suggest selection rule breakdown for the A_{1u} totally forbidden mode causing the appearance of the extra modes.

We adopt a perturbation theory approach. It must be stressed at the outset though, that the large strengths of the forbidden modes suggests that structural changes near the surface are probably not "small." To be concrete we choose as a working example the case of most interest. Let $|A_{1u}\rangle$ represent a state of the crystal where one of the type A_{1u} forbidden modes at $k=0$ has one quantum excited and all other modes are not excited. Similarly, let $|E_u\rangle$ be a state with one quantum of excitation in one of the $E\perp C$ axis infrared modes. If

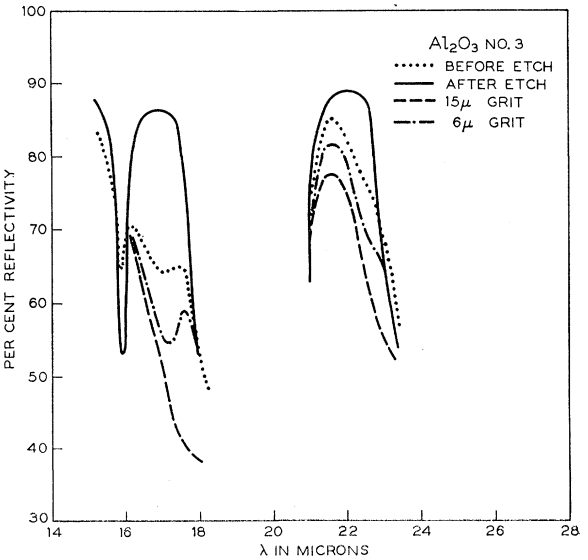

FIG. 6. Reflectivity of Al_2O_3 for $E\perp C$ axis measured after various surface treatments. The dotted curve was measured for the "as-received" crystal and probably corresponds to a 1-μ grit finish.

[15] M. Born and K. Huang, *Dynamical Theory of Crystal Lattices* (Clarendon Press, Oxford, 1954), Chap. II.

TABLE IV. Perturbation of Al_2O_3 modes.

Unperturbed initial mode		Perturbation potential H'	Resulting modes	Comments
		Symmetry type of:		
A_{1u}	×	E_g	$=E_u$	2 A_{1u} allowed in $\perp$
A_{1g}	×	E_u	$=E_u$	2 Raman allowed in $\perp$
A_{2g}	×	E_u	$=E_u$	3 A_{2g} allowed in $\perp$
E_g	×	E_u	$=A_{1u}+A_{2u}+E_u$	5 Raman allowed in $\parallel$ and $\perp$
A_{2u}	×	E_g	$=E_u$	$\parallel$ allowed in $\perp$

the perturbation H' is applied to the crystal, $|A_{1u}\rangle$ becomes active in the $E\perp C$ spectrum if

$$a_{E_u}=\frac{\langle E_u|H'|A_{1u}\rangle}{W(A_{1u})-W(E_u)} \text{ is not zero.}$$

The reason for the mode becoming active is simply that the coefficient a_{E_u} expresses the amount of $|E_u\rangle$ wave function mixed into the $|A_{1u}\rangle$ state. Since $|E_u\rangle$ has net dipole moment, the new state will now have it also and thus will be able to interact with the infrared electric field. Group theory can now give us the selection rules for this type of induced activity. The basic theorem on matrix elements states that if the A_{1u} representation times the representation H' transforms by, contains the E_u representation, then a_{E_u} is *not* restricted to be zero by symmetry.

Proceeding with the example, we use some hindsight and consider a perturbation H' that has the transformation properties of the irreducible representation E_g. By using Table III and multiplying the rows in the usual way, we find $A_{1u}\times E_g=E_u$. Since the product *does* contain the E_u representation, a type E_g perturbation does allow the A_{1u} modes to be active in the $E\perp C$ spectrum.

Since any conceivably perturbation must transform according to one or more of the irreducible representations, an examination of all possible cases can be done very quickly. The only cases which lead to infrared activity for $E\perp C$ axis are listed in Table IV.

Table IV shows that an E_g type strain or perturbation of the lattice allows the two forbidden A_{1u} modes to appear. An E_u type perturbation allows a total of ten modes to appear in the $E\perp C$ spectrum. We rule out then the possibility of an E_u type perturbation being present in the samples studied because we observe only two forbidden modes. There are two additional weaker arguments against the E_u perturbation. None of the Raman frequencies[3] agrees with the frequency of the 598 cm^{-1} forbidden mode, and an E_u type strain would be nonuniform.

The last entry in Table IV shows that an E_g strain which can cause the two observed modes, can also cause the infrared vibrations parallel to the C axis to appear in the perpendicular spectrum. The forbidden modes we observe most clearly (sample 1) are at 16.7 and 22.3 μ. The $E\|C$ infrared modes are at 17.1 and 25.0 μ. It appears very unlikely that the 22.3 μ forbidden mode is actually an $E\|C$ infrared mode because of the large frequency difference. We therefore suggest that it is an A_{1u} mode. Since the two A_{1u} modes involve similar atomic motions, it appears reasonable that both forbidden modes which are observed are of the A_{1u} type. That is, we suppose that an E_g type strain couples the E_u type wave function more efficiently into the A_{1u} rather than the A_{2u} wave function.

The E_g representation is two dimensional. It has two basis functions which transform as x^2-y^2 and $2xy$ (where x and y are two orthogonal axes perpendicular to the crystalline C axis). Strains which transform like these basis functions are shears, and are, of course, equivalent within a coordinate transformation which rotates the x-y plane. Because of the equivalence we continue to discuss only the x^2-y^2 type strain.

We can now form a picture of the ion motions that cause the forbidden modes. In so doing, we will be able to show why the forbidden modes appear only for $E\perp C$ spectra taken on certain crystal faces. The A_{1u} modes involve the vibration of oxygen ions at the vertices of an equilateral triangle as shown in Fig. 7.[14] All oxygen triangles are perpendicular to the C axis. The A_{1u} modes

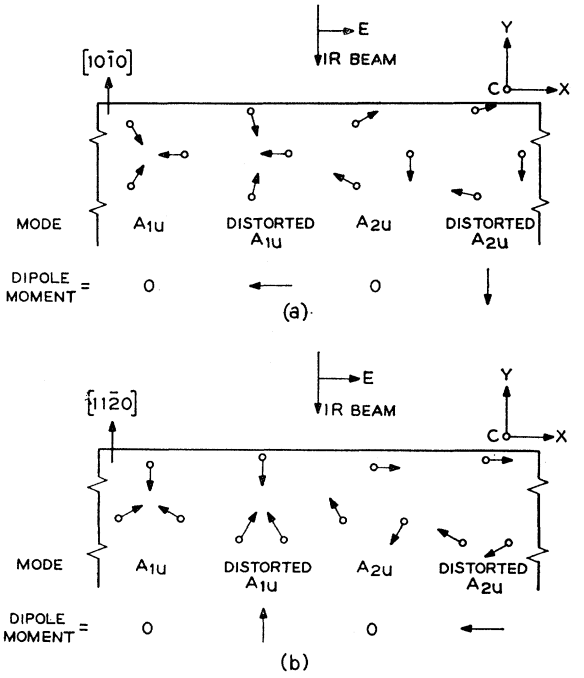

FIG. 7. Schematic representation of the important motions in the A_{1u} and A_{2u} mode . The Al_2O_3 crystal is taken to be a semi-infinite slab with the C axis extending out of the page. The open circles represent the equilibrium positions of the oxygen ions. Both normal and sheared regions are shown in the same crystal for the sake of comparison of the effect of shear on the ion motions. Part (a) shows the oxygen ion behavior near a (10$\bar{1}$0) face and Part (b) near a (11$\bar{2}$0) face which is 30° away. The infrared beam is polarized to detect $E\perp C$ modes only.

are infrared inactive because no net dipole moment is generated by the motion. The mode is Raman inactive also because while there may be some polarizability change due to the close approach of the oxygens in the triangle depicted, there is a canceling effect elsewhere in another oxygen triangle in the primitive cell. An x^2-y^2 type distortion will upset the balance of dipole moments for the A_{1u} vibrations as shown in Fig. 7. Infrared absorption can now occur at the A_{1u} mode frequency for the infrared electric vector polarized along the x direction of Fig. 7(a) ($E\perp C$).

Figure 7 also illustrates the oxygen ion motion for one of the A_{2u} modes. It is only necessary to show this particular A_{2u} mode since the others either occur at zero frequency (acoustic mode) or involve oxygen ion motion parallel to the C axis. When we apply an x^2-y^2 type distortion to the A_{2u} mode shown, it develops vibrating dipole moment perpendicular to the C axis. We note, however, that this dipole moment is always perpendicular to that of the perturbed A_{1u} mode. When this latter fact was realized, the samples were x rayed to determine the actual orientation of the oxygen triangles relative to the surfaces used for the infrared measurements. Sample 1 was found to be within 4° of the orientation shown in Fig. 7(a). Thus, the position of the oxygen ions favors the appearance of the A_{1u} forbidden modes in the infrared spectrum. Sample 3 was found to be 15° away from the orientation shown in Fig. 7(a), which means that the oxygen triangle positions relative to the surface are half way between the orientations shown in Figs. 7(a) and 7(b). Since we see little if any sign of the A_{2u} modes in the $E\perp C$-axis spectrum, it appears that these modes are coupled much less strongly to the $E\perp C$ modes by the shear-strain field.

We picture the A_{1u} forbidden modes appearing as follows. An Al_2O_3 crystal with mechanically polished faces has considerable strain near the surface. The free surface perpendicular to a y axis (or at least *not* perpendicular to the C axis) plays the decisive role.[16] Since a free surface relieves all perpendicular stress, this surface treats x and y directions differently causing an x^2-y^2 type strain to be large, thus causing infrared absorption by the A_{1u} modes near this surface only. This picture is thus consistent with the symmetry arguments and with the observation that forbidden modes never appear on surfaces perpendicular to the C axis.

SUMMARY

Classical oscillator analysis of the reflection spectra of several α-Al_2O_3 samples has yielded the frequencies, strengths, and linewidths of the infrared-active modes predicted by group theory. The frequencies of six longitudinal phonon branches near $k=0$ have also been determined. Optical constants such as n, k, α, ϵ' and ϵ'' may be obtained for any frequency in the infrared range by inserting the mode parameters listed in Table II into the appropriate formulas.

Many forbidden modes have been observed. The two strongest are related to surface damage. The strength of these modes may actually be used as an indication of surface perfection. A perturbation theory analysis shows that these modes are probably A_{1u} type lattice vibrations which cannot normally be detected by infrared or Raman methods. Their appearance is associated with the distortion of the oxygen triangles of the α-Al_2O_3 structure.

ACKNOWLEDGMENTS

The author is indebted to L. E. Howarth and A. Contaldo for the infrared measurements. It is a pleasure to acknowledge helpful discussions with Dr. D. E. McCumber.

[16] The question arises as to whether this surface region is a second phase of Al_2O_3 with a unique structure. To determine whether the oxygen triangle distortion is constant over macroscopic regions of the surface, different experiments must be done since the infrared results are insensitive to the sign of the distortion.